MIT Libraries | DSpace@MIT

MIT Open Access Articles

Immersion Freezing of Kaolinite: Scaling with Particle Surface Area

The MIT Faculty has made this article openly available. ***Please share*** how this access benefits you. Your story matters.

Citation: Hartmann, Susan et al. "Immersion Freezing of Kaolinite: Scaling with Particle Surface Area." Journal of the Atmospheric Sciences 73.1 (2016): 263–278. © 2016 American Meteorological Society

As Published: http://dx.doi.org/10.1175/jas-d-15-0057.1

Publisher: American Meteorological Society

Persistent URL: http://hdl.handle.net/1721.1/105725

Version: Final published version: final published article, as it appeared in a journal, conference proceedings, or other formally published context

Terms of Use: Article is made available in accordance with the publisher's policy and may be subject to US copyright law. Please refer to the publisher's site for terms of use.

Massachusetts Institute of Technology

Immersion Freezing of Kaolinite: Scaling with Particle Surface Area

SUSAN HARTMANN, HEIKE WEX, TINA CLAUSS, AND STEFANIE AUGUSTIN-BAUDITZ

Department of Experimental Aerosol and Cloud Microphysics, Leibniz Institute for Tropospheric Research, Leipzig, Germany

DENNIS NIEDERMEIER

Department of Physics, Michigan Technological University, Houghton, Michigan, and Department of Experimental Aerosol and Cloud Microphysics, Leibniz Institute for Tropospheric Research, Leipzig, Germany

MICHAEL RÖSCH

Department of Earth, Atmospheric and Planetary Sciences, Massachusetts Institute of Technology, Cambridge, Massachusetts, and Department of Experimental Aerosol and Cloud Microphysics, Leibniz Institute for Tropospheric Research, Leipzig, Germany

FRANK STRATMANN

Department of Experimental Aerosol and Cloud Microphysics, Leibniz Institute for Tropospheric Research, Leipzig, Germany

(Manuscript received 27 February 2015, in final form 9 September 2015)

ABSTRACT

This study presents an analysis showing that the freezing probability of kaolinite particles from Fluka scales exponentially with particle surface area for different atmospherically relevant particle sizes. Immersion freezing experiments were performed at the Leipzig Aerosol Cloud Interaction Simulator (LACIS). Size-selected kaolinite particles with mobility diameters of 300, 700, and 1000 nm were analyzed with one particle per droplet. First, it is demonstrated that immersion freezing is independent of the droplet volume. Using the mobility analyzer technique for size selection involves the presence of multiply charged particles in the quasi-monodisperse aerosol, which are larger than singly charged particles. The fractions of these were determined using cloud droplet activation measurements. The development of a multiple charge correction method has proven to be essential for deriving ice fractions and other quantities for measurements in which the here-applied method of size selection is used. When accounting for multiply charged particles (electric charge itself does not matter), both a time-independent and a time-dependent description of the freezing process can reproduce the measurements over the range of examined particle sizes. Hence, either a temperature-dependent surface site density or a single contact angle distribution was sufficient to parameterize the freezing behavior. From a comparison with earlier studies using kaolinite samples from the same provider, it is concluded that the neglect of multiply charged particles and, to a lesser extent, the effect of time can cause a significant overestimation of the ice nucleation site density of one order of magnitude, which translates into a temperature bias of 5–6 K.

1. Introduction

Ice formation in clouds influences the formation of precipitation, cloud radiative properties, and cloud lifetime and therefore impacts both Earth's weather and climate (e.g., DeMott et al. 2003a; Lohmann 2006). Primary ice formation occurs either through homogeneous or heterogeneous ice nucleation. The latter process is catalyzed by a foreign substance called ice nucleating particle (INP) and occurs at higher temperature or lower supersaturation than those observed in the case of homogeneous ice nucleation. In the framework of this paper, we focus on immersion freezing, which is defined as heterogeneous ice nucleation process in supercooled droplets, where the ice nucleation takes place directly at the surface of the INP. Results gained from field

Denotes Open Access content.

Corresponding author address: Susan Hartmann, Department of Experimental Aerosol and Cloud Microphysics, Leibniz Institute for Tropospheric Research, Permoserstr. 15, Leipzig 04318, Germany. E-mail: hartmann@tropos.de

DOI: 10.1175/JAS-D-15-0057.1

© 2016 American Meteorological Society

studies such as Ansmann et al. (2009), Westbrook and Illingworth (2011), and de Boer et al. (2011) indicate that immersion freezing is a very important mechanism for ice formation in atmospheric mixed-phase clouds.

Mineral dust particles were found to cause glaciation of supercooled clouds (DeMott et al. 2003b; Sassen et al. 2003; Mahowald and Luo 2003; Seifert et al. 2010). Analyses of ice crystal residues indicate that mineral dusts contribute to atmospheric INPs (Kumai 1961; DeMott et al. 2003b; Twohy and Poellot 2005; Richardson et al. 2007; Mertes et al. 2007; Pratt et al. 2009; Kamphus et al. 2010). Atmospheric mineral dust is found in different particle sizes ranging from a few hundred nanometers to several tenths of micrometers (Maring et al. 2003; Kaaden et al. 2009; Kandler et al. 2009). Depending on the source region, airborne mineral dust is made up of complex mixtures of different particle sizes, morphologies, and mineral phases (Glaccum and Prospero 1980; Ganor 1991; Avila et al. 1997; Blanco et al. 2003; Kandler et al. 2007). The clay fraction is about half of the atmospheric mineral dust and in particular the fraction of kaolinite is in a range of 7%–41% (Johnson 1976; Ganor and Mamane 1982; Chester et al. 1984; Arnold et al. 1998; Kandler et al. 2011; Murray et al. 2012). Submicron kaolinite particles contribute significantly to atmospheric mineral dust particulate matter and research on its ice nucleation ability is of great interest.

From laboratory studies, kaolinite can be considered as a well-known proxy for mineral dust and has been analyzed quite often since the 1960s. Early laboratory studies from Mason and Maybank (1958), Mason (1960), Hoffer (1961), and Pitter and Pruppacher (1973) examined ice nucleation caused by mineral dust particles immersed in droplets and observed discrepancies in the freezing temperatures. In more recent experiments, improvements could be achieved as the particle surface area was determined and taken into account for the interpretation of the immersion freezing results (Connolly et al. 2009; Niedermeier et al. 2010; Sullivan et al. 2010; Niedermeier et al. 2011b; Augustin-Bauditz et al. 2014; Zolles et al. 2015). Other experiments examined the immersion freezing of droplets with varying particle sizes or particle loads: Archuleta et al. (2005), Marcolli et al. (2007), Welti et al. (2009), Lüönd et al. (2010), Welti et al. (2012), and Pinti et al. (2012) reported an increasing freezing probability with increased available particle surface area. In other words, the dependence of immersion freezing on the particle surface area was shown on a qualitative basis. For the quantification of the particle surface area dependence, often quantities are used that are independent of particle sizes or particle loads immersed in the droplets. Such quantities are, for example, the ice nucleation surface site density or the heterogeneous ice nucleation rate coefficient following the singular or stochastic approach, respectively. In the reviews of Murray et al. (2012), Hoose and Möhler (2012), the study of Knopf and Alpert (2013), and Hiranuma et al. (2015) the spread of these quantities reported was usually greater than or equal to two orders of magnitude at similar conditions. A better agreement of surface area conserved quantities could be achieved in Niemand et al. (2012), Murray et al. (2011), and Atkinson et al. (2013). In Niemand et al. (2012) immersion freezing experiments were performed with polydisperse aerosol using measured particle size distributions to determine the total particle surface area. There, it has to be assumed that aerosol composition and surface properties do not vary with particle size. This needs to be proven, as the ice nucleation properties of the sample investigated might differ for different particle sizes [recommended in the study of Niemand et al. (2012) and Hoose and Möhler (2012)]. Murray et al. (2011) analyzed the immersion freezing of KGa-1b kaolinite from the Clay Minerals Society (CMS) with the cold-stage method, where typically multiple particles are immersed in the droplets. In this context, Murray et al. (2011) also speculated that ''one kaolinite particle has very similar or identical ice nucleating properties to another kaolinite particle and kaolinite particles of the same size have the same probability of nucleating ice under a given set of conditions. This now needs to be tested on a single particle basis.'' In contrast, Broadley et al. (2012), using a similar method as Murray et al. (2011) with a different clay mineral, an illite sample, found only for low surface areas immersed in the droplets that the medium freezing temperature depended on particle surface area. From this, they concluded that a strong particle-to-particle variation in terms of ice nucleation ability exists. Additionally, from Pinti et al. (2012) we learn that different dusts and even different types of kaolinite behave differently concerning their ice nucleation properties. By doing size-selected measurements at different atmospherically relevant particles sizes, it can be examined if differently sized particles possess similar ice nucleation properties and if distinct particle-to-particle variations exist for the here-analyzed kaolinite.

Furthermore, air-suspended droplets with one particle per droplet acting as INP are more atmospherically relevant. Already Marcolli et al. (2007) suggested to study the immersion freezing of only one up to a very few particles per droplet. Following Murray et al. (2012), the analysis of air-suspended droplets avoids any potential interference due to nucleation by the substrate.

In the here-presented study, to experimentally prove the scaling of the freezing probability with particle surface area in the immersion mode, which is presumed in the ice nucleation theory, we use the following experimental conditions: quasi-monodisperse particles, separate examination of different particle sizes, and air-suspended droplets in which only a single particle is immersed. For that, we investigate the immersion freezing ability of quasi-monodisperse kaolinite particles as a function of temperature and particle size at the Leipzig Aerosol Cloud Interaction Simulator (LACIS; Stratmann et al. 2004; Hartmann et al. 2011). In the first step, we analyze the independence of immersion freezing on droplet volume. This is a necessary condition for the following step. In that, we attempt to receive better-constrained values for particle-surface-independent quantities and hence study the scaling of the freezing probability in the immersion freezing mode very thoroughly.

A similar approach was already applied by Lüönd et al. (2010), Welti et al. (2012), and Wex et al. (2014). However, these studies did not take any effects of multiply charged particles into account, as they can appear when using the differential mobility analyzer (DMA) technology for particle size selection. Multiply charged particles are larger with respect to particle size than singly charged particles and hence they have larger surface areas, which might influence the freezing probability.

2. Material and experimental setup

LACIS is a laminar flow tube that allows for the investigation of immersion freezing of well-characterized, size-selected particles, where only one particle is immersed in each droplet under well-defined thermodynamic conditions. In the present study, the immersion freezing potential of kaolinite provided by Fluka (Sigma-Aldrich) was investigated. Kaolinite belongs to the clay minerals and is a two-layer phyllosilicate with alternating SiO_4-tetrahedron and $Al(OH)_8$-octahedron structures, which originate from chemical weathering of, for example, feldspar. In Atkinson et al. (2013), using X-ray diffraction, the following composition of Sigma-Aldrich kaolinite was given: 83 wt% kaolinite, 6 wt% quartz, 5.5 wt% illite/mica, and 4.5 wt% K-feldspar. The generation of airborne kaolinite for our experiment as well as the experimental setup (Fig. 1) will be described in the following.

a. Particle generation

The particle-generation procedure used in this study was similar to that already described in Niedermeier et al. (2010, 2011b) and the main functional principle is briefly repeated in the following. At first, the kaolinite powder was dispersed by means of a fluidized bed generator (TSI 3400A, TSI Inc., St. Paul, Minnesota). Because of multiple collisions and arising friction effects in the generator, the air-suspended kaolinite particles were multiply charged. To partially discharge the particles, a self-built Corona discharger was used. A cascade impactor [Micro-Orifice Uniform-Deposit Impactor (MOUDI), Model 100R, MSP Corporation, Shoreview, Michigan] with different possible impaction plate configurations was used to remove larger particles from the aerosol. When selecting particles with a mobility diameter of 300 nm, particles with aerodynamic particle diameters larger than 560 nm were removed from the aerosol in the MOUDI with a cutoff efficiency of around 50%. In the case of particles with 700-nm electric mobility particles, particles larger than 1000-nm aerodynamic particle diameter were removed. The application of the MOUDI did not ensure the removal of all large particles, which is discussed in section 4. Afterward, a Krypton 85 neutralizer was used to establish a bipolar equilibrium charge distribution on the aerosol particles. To select a quasi-monodisperse particle size fraction from the aerosol, a DMA (Knutson and Whitby 1975) of type "Vienna medium" was used

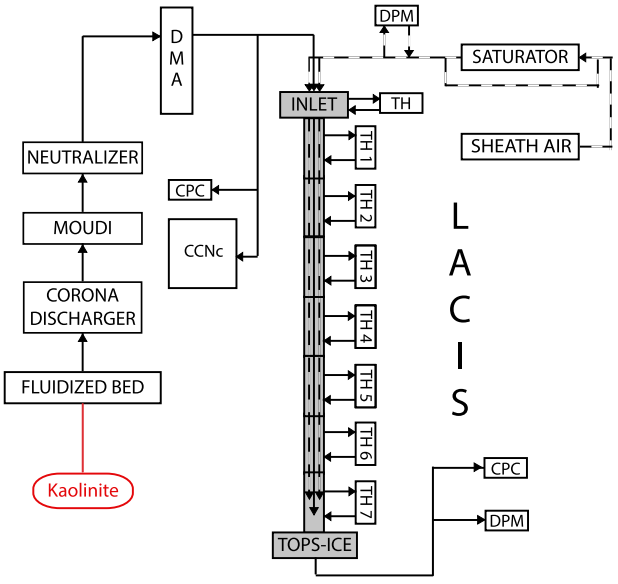

FIG. 1. Schematic flow diagram of the experimental setup, including particle generation, cloud droplet activation measurement, and the laminar diffusion cloud chamber LACIS. Components include Micro-Orifice Uniform-Deposit Impactor (MOUDI), differential mobility analyzer (DMA), condensational particle counter (CPC), cloud condensation nucleus counter (CCNc), dewpoint mirror (DPM), thermostat (TH), and Thermo-stabilized Optical Particle Spectrometer for ice particle detection (TOPS-Ice).

for particle sizes up to 800 nm. Alternatively, a custom-built Maxi-DMA (Leinert 2002; Raddatz et al. 2013) in combination with an upstream cyclone impactor with adjustable cutoff diameter was installed in order to generate quasi-monodisperse particles of 1000 nm. A DMA in general is a cylindrical capacitor that can be used for the classification of charged aerosol particles according their electric mobility. With this size selection method, we are able to examine particles with known size (mobility diameter). This enables a determination of the particle surface area, a parameter that is expected to be of importance for ice nucleation. Finally, the aerosol flow containing quasi-monodisperse particles with typical number concentrations in a range of 50–100 cm^{-3} was split to feed into a cloud condensation nucleus counter (DMT; Roberts and Nenes 2005), a condensation particle counter (CPC, TSI 3010), and LACIS.

b. CCN counter

The quasi-monodisperse aerosol particles were analyzed according to their activity to act as cloud condensation nuclei (CCN) by the means of a CCN counter. For that, the flow containing the quasi-monodisperse particle was split and sent to the CCN counter and a condensation particle counter to measure total particle number concentration of condensation nuclei (CN). The ratio of CCN to CN determines the activated fraction.

c. LACIS

The laminar flow tube LACIS (Stratmann et al. 2004) has a top-to-bottom flow direction and consists of seven 1-m-long tube sections with an internal diameter of 15 mm. Each tube section can be temperature controlled separately by a thermostat. Humidified particle-free sheath air and the aerosol with flow rates of 4.0 and 0.8 L min^{-1}, respectively, enter LACIS in an isokinetic fashion. Thereby, a particle beam is formed with a diameter of 2 mm at the center of the flow tube being surrounded by the sheath air. As a function of the inlet dewpoint and the inlet temperature of the entering air and the wall temperature of the tube sections, a temperature and saturation profile is established along the tube due to heat and vapor diffusion processes. All particles moving along the centerline of the laminar flow tube experience the same humidity and temperature conditions. Detailed information explaining the operational principle of LACIS in the immersion freezing mode is presented in Hartmann et al. (2011).

In this study, the immersion freezing experiments were performed in the following mode: all aerosol particles were activated to droplets that subsequently grow. Further cooling leads to the onset of immersion freezing. As a result, a certain droplet fraction freezes for an ice nucleation time of 1.6 s.

d. Particle detection

At the outlet of LACIS, the Thermo-stabilized Optical Particle Spectrometer for the detection of ice (TOPS-Ice; Clauss et al. 2013) was used to analyze the phase state of the hydrometeors. The phase-state distinction takes place via the evaluation of the polarization state of scattered light; for further details, see Clauss et al. (2013). Therefore, by means of TOPS-Ice it can be distinguished between unfrozen and frozen droplets. This allows for the determination of the size of the unfrozen droplets and the ice fraction, which is defined as the number of frozen droplets to the total number of frozen and unfrozen droplets. The ice fraction could be derived in a range from 10^{-2} to 1 for the kaolinite particles investigated.

3. Droplet volume independence

Heterogeneous ice nucleation is generally assumed to be a process depending on the surface area of the INP. However, in the literature, inconsistent views can be found. In some laboratory and modeling studies (e.g., Bigg 1953; Hoffer 1961; Pitter and Pruppacher 1973; Pruppacher and Klett 1997; Diehl and Mitra 1998; Diehl et al. 2002; Diehl and Wurzler 2004; Diehl et al. 2006), it was assumed that immersion freezing is droplet-volume dependent, while other more recent laboratory studies (e.g., Marcolli et al. 2007; Welti et al. 2009; Lüönd et al. 2010; Murray et al. 2011; Welti et al. 2012; Broadley et al. 2012) assumed that immersion freezing depends on the particle surface area of the immersed particles instead of on the droplet volume. Experimental studies claiming a droplet volume dependence generally examined droplets produced from a suspension. We speculate that the assumption of a droplet volume dependence results from the fact that for a constant concentration of the suspension, larger droplets contain more particles and hence have a higher available particle surface area, which causes an increased freezing probability.

Moreover, homogeneous ice nucleation is droplet-volume dependent, because the formation of a critical ice cluster inducing freezing of the droplet depends on kinetic effects and water molecule availability. Because of the presence of a substrate, the heterogeneous ice nucleation is energetically preferred as critical cluster formation takes place directly at the surface of the INP, although the exact mechanism is still unclear (e.g., Hoose and Möhler 2012). Therefore, it is reasonable that immersion freezing depends on particle surface area and not on droplet volume. However, this is a

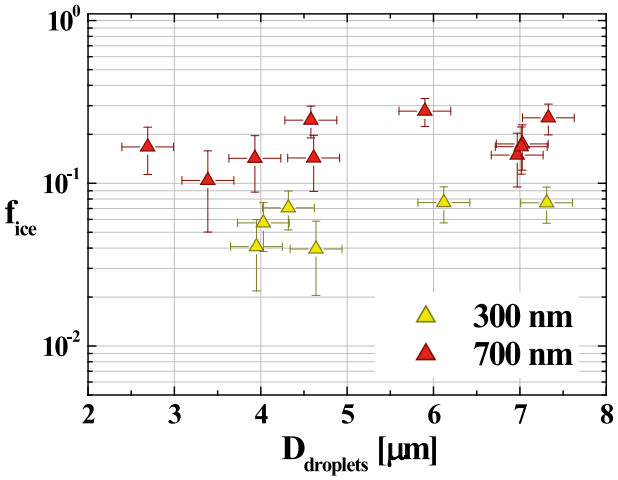

FIG. 2. Ice fraction as a function of droplet diameter for kaolinite particles with mobility diameters of 300 and 700 nm at −35°C. For each data point, at least 2000 droplets were examined. Each droplet contains only one kaolinite particle and all particles have similar sizes.

necessary condition that needs to be demonstrated for further investigations in regard to the scaling of the freezing probability with particle surface area.

The inconsistent views are an example of mistaking relation and causality. Of course there is a relation between freezing probability and droplet volume assuming constant particle concentration of the suspension, but the causation is determined owing to the particle surface area in the droplets. To our knowledge, so far no measurements exist that quantify both the droplet volume and particle surface area dependence very thoroughly. In the following paragraph, we will elaborate that the freezing probability of immersion freezing does not depend on the droplet volume.

The analysis was performed for 300- and 700-nm quasi-monodisperse particles with respect to mobility size at LACIS. The droplet size was controlled by varying the saturation with respect to water. The results are shown in Fig. 2. With increasing droplet sizes from 1.5 to 7.5 μm in diameter (i.e., a factor of 125 in droplet volume), the ice fractions are constant for 300- and 700-nm kaolinite particles, respectively, taking the measurement uncertainties into account. The increase in particle size and hence in particle surface area leads to an increased ice fraction though. This shows that the freezing of droplets containing a single INP does not depend on droplet volume in the range of droplet sizes investigated.

Alpert et al. (2011) and Rigg et al. (2013), studying other ice nucleating materials than mineral dust, also could show that the freezing temperatures did not depend on the droplet volume. In particular, in the study of Alpert et al. (2011) the ice nucleation behavior of marine diatoms immersed in aqueous NaCl droplets was analyzed for a droplet size range of several tens of micrometers in diameter. Similar investigations concerning the volume independence of immersion freezing were performed in Rigg et al. (2013) for aqueous ammonium sulfate droplets containing humiclike substances. However, to our knowledge the independence of immersion freezing on droplet volume when keeping particle surface area constant was shown for the first time in the present study with this high accuracy and precision of the measurement method (i.e., one quasi-monodisperse particle per droplet and similar droplet sizes). In the following, the effect of particle surface area on the freezing probability will be examined more closely.

TABLE 1. Size and fraction of singly and multiply charged particles of the resulting aerosol after size selection.

	Mobility size (nm)		
	300	500	700
Size of doubly charged particles (nm)	507	889	1277
Size of triply charged particles (nm)	707	—	—
Fraction of singly charged particles	0.44	0.64	0.88
Fraction of doubly charged particles	0.35	0.36	0.12
Fraction of triply charged particles	0.21	—	—

4. Determination of multiply charged particles

As mentioned above, utilizing a DMA for particle size selection, multiply charged particles can occur. These particles are larger than singly charged particles of the same mobility, which might influence the ice nucleation probability significantly. Particles are selected according to their electric mobility if a DMA is used (Knutson and Whitby 1975). For example, the following particles have the same electrical mobility (electrical mobility diameter): singly charged particles with a Stokes diameter of 300 nm, doubly charged particles with a Stokes diameter of 507 nm, and triply charged particles with a Stokes diameter of 707 nm (Table 1).

To determine the fraction of multiply charged particles, the kaolinite particles were examined with respect to their ability to nucleate cloud droplets using the CCN counter, together with the CPC. Particles of a constant size, selected with the DMA as described above, were fed into the CCN counter and the CPC simultaneously. The supersaturation inside the CCN counter was changed stepwise, and at each supersaturation the activated fraction (AF), which is the ratio of CCN to CN, was determined. The curves obtained for particles with electrical mobility diameters of 300, 500, and 700 nm are shown in Fig. 3 (top panel).

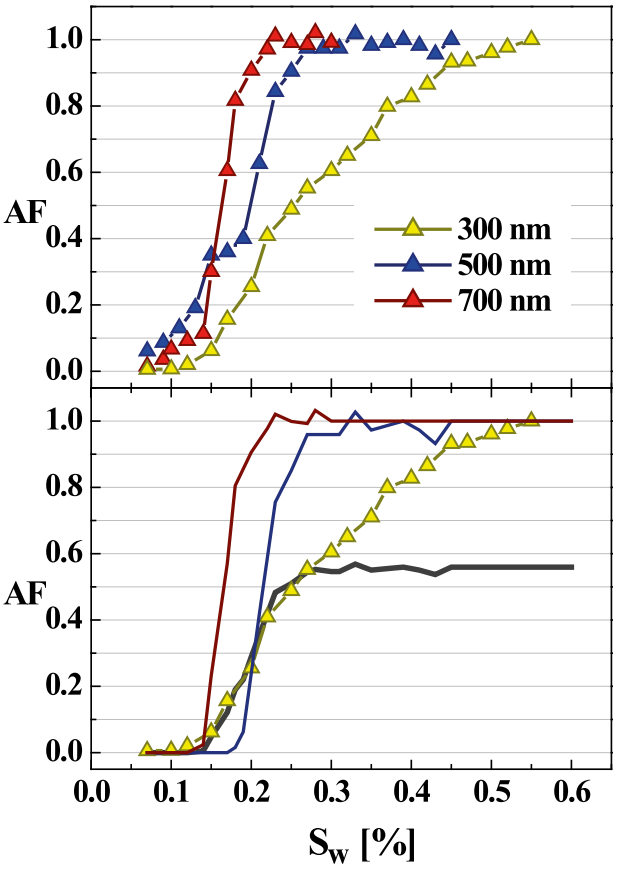

FIG. 3. Activated fraction at different supersaturations. (top) Measured AF curves for 300, 500, and 700 nm. (bottom) Yellow curve is as in the top panel, and dark blue and dark red curves are activated fraction curves for 500 and 700 nm, respectively, from which the doubly charged particles were subtracted. The black curve is the sum ($a_{500}AF_{500} + a_{700}AF_{700}$) with 0.35 and 0.21 for a_{500} and a_{700}, respectively.

For particle sizes of 500- and 700-nm electrical mobility diameter, a plateau in the activated fraction at low supersaturations can be seen in the range of supersaturations from 0.15% to 0.2% and from 0.1% to 0.15%, respectively. These plateaus indicate the presence of doubly charged particles, and from the plateaus, the fraction of doubly charged particles can be determined to be 36% and 12% for 500 and 700 nm, respectively (see Table 1). In a former study using the identical particle generation setup, we performed the same analysis for 300-nm ATD particles and, in that case, only a negligible amount of doubly charged particles was found. However, in this study the amount of multiply charged particles is higher and hence it has to be accounted for.

The bottom panel of Fig. 3 displays the activated fraction curves of the 500- and 700-nm particles from which the doubly charged particles were subtracted and that were afterward normalized to a maximum AF of 1. The activated fraction curve for the particles with an electrical mobility diameter of 300 nm is very broad, indicating that multiply charged particles are present in the aerosol. As these Stokes diameters are close to 500 and 700 nm (see Table 1), we determined the fraction of doubly and triply charged 300-nm particles as follows: the activated fraction curves of the 500- and 700-nm particles as shown in the bottom panel of Fig. 3 and the measured activation curve for the 300-nm particles were all interpolated so that data existed in a resolution of 0.01% with respect to supersaturation. All 500- and 700-nm particles were activated for supersaturations above 0.3%, and hence, in the following, only the range of supersaturations up to 0.29% was considered. Assuming now a mixture of multiply charged particles having the same electric mobility, AF for the particles with 300-nm mobility diameter (AF_{300}^{mob}) can be expressed as a function of supersaturation with respect to water S_w:

$$AF_{300}^{mob}(S_w) = a_{300}AF_{300}(S_w) + a_{500}AF_{500}(S_w) + a_{700}AF_{700}(S_w), \quad (1)$$

with a_i and AF_i being the fraction of singly or multiply charged particles of the resulting aerosol after size selection and the activated fractions of respective particle size, respectively. Based on Eq. (1), a least squares fit was made to obtain a_{500} and a_{700} by assuming that $AF_{300} = 0$ below 0.29% supersaturation. The resulting values are 35% and 21%, respectively (Table 1), and the accordant sum of nonsingly charged particles is shown as black curve in the bottom panel of Fig. 3. The yellow curve in this panel is again the activated fraction measured for the particles with an electrical mobility diameter of 300 nm, and the good agreement between the black and yellow curves up to a supersaturation of 0.3% (i.e., an activated fraction of roughly 55%) indicates that indeed if selecting 300-nm particles with the DMA, a large fraction of the selected particles were doubly and triply charged particles.

In the following, we will account for the external mixture of singly, doubly, and triply charged kaolinite particles, based on the fractions as given in Table 1.

5. Particle surface area dependence

Figure 4 depicts the ice fraction f_{ice} as a function of temperature T for kaolinite particles with mobility diameters of 300 (yellow triangle), 700 (red triangle), and 1000 nm (black dots) and the homogeneous freezing curve of highly diluted ammonium sulfate solution droplets (open blue squares). The measurement uncertainties given are the temperature uncertainties of ±0.3 K and the uncertainties of f_{ice} that correspond to single standard

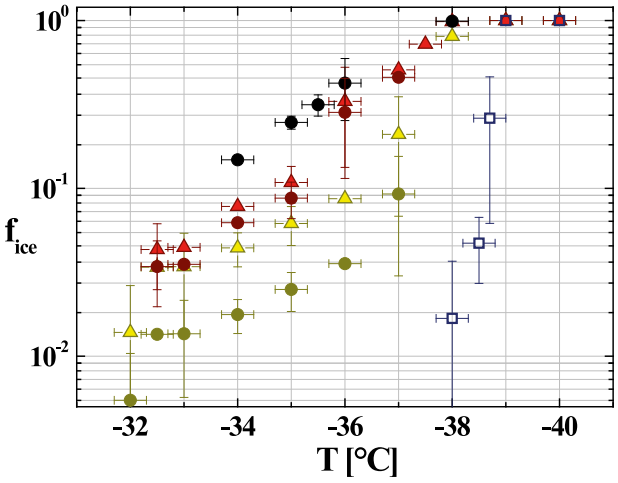

FIG. 4. Ice fraction as a function of temperature for different kaolinite particle sizes of 300 (light and dark yellow), 700 (light and dark red), and 1000 nm (black). The triangles (lighter colors) denote charge-uncorrected ice fractions and the dots (darker colors) present charge-corrected ones. Additionally, the homogeneous freezing of highly diluted ammonium sulfate solution droplets is given (open blue squares).

deviations of the average from at least three measurements. Homogeneous ice nucleation has to be accounted for at temperature values below −37.5°C and becomes dominant with decreasing temperature. In a higher temperature range where immersion freezing is the dominating ice nucleation process, kaolinite particles act as INPs with the largest particles (1000 nm) being most efficient. The 700-nm kaolinite particles produce less ice, and the smallest ice fractions are found for 300-nm kaolinite particles. In Fig. 4, it can be seen that the ice fractions increase exponentially with temperature and show a similar temperature dependence for different particle sizes right up to the homogeneous freezing limit, as the curves for the three different sizes of kaolinite particles are parallel to each other. Both results hint at similar ice nucleation properties of differently sized kaolinite particles. This finding is similar to that of Murray et al. (2011) for kaolinite provided by the Clay Minerals Society.

a. *Time-independent description*

To quantify the particle surface area dependence on immersion freezing, first, a time-independent approach based on the ice nucleation surface site density will be applied. We consider the immersion freezing in the view of the singular approach [e.g., according to Levin (1950) and Langham and Mason (1958)]. The critical ice cluster, which initiates freezing of the droplet, forms on specific sites on the surface of an INP at a specific characteristic temperature T. Following, for example, Murray et al. (2012), the probability of freezing in terms of ice fraction can be described as

$$f_{\text{ice}}(T) = 1 - \exp[n_s(T)s_p], \tag{2}$$

with the ice nucleation surface site density n_s, which is defined as a temperature-dependent number of ice nucleation sites per particle surface area s_p.

The aerosol in our case is composed of singly and multiply charged particles and is, hence, also a mixture of different discrete surface areas (discussed in section 4). At this point, it is worth mentioning that the electric charge itself does not matter for the ice nucleation behavior in the here-presented study. As the objective here is to study the effect of surface area on the ice nucleation efficiency, the presence of particles with different sizes, which we refer to as an external mixture, has to be accounted for. To derive n_s, multiply charged particles for 300 and 700 nm had to be considered. The 1000-nm kaolinite particles contain a negligible number of multiply charged particles. The ice fraction of the droplet population with externally mixed INPs can be described by the superposition of the ice fraction of the subpopulation weighted by their fraction of occurrence a_i:

$$f_{\text{ice}}(T) = \sum_{i=1}^{n} a_i f_{\text{ice},i}(T), \tag{3}$$

with $f_{\text{ice},i}(T) = 1 - \exp[-n_{s,i}(T)s_{p,i}]$. The derivation and explanations of Eq. (3) can be found in the appendix in detail. The fraction a_i of singly or multiply charged particles of the resulting aerosol after size selection is derived from the CCN measurements as discussed in section 4. The particle surface area was calculated assuming a spherical shape of the particles. Then n_s was obtained separately for each selected size (i.e., for 300, 700, and 1000 nm) and temperature by using Eq. (3). To do so, at each selected size, it had to be a priori assumed that n_s for the differently sized particles was identical.

This resulted in three separate datasets for n_s that all fall together; see Fig. 5. In fact, the conserved quantity n_s is no function of particle size or rather particle surface area. For this reason, we found strong indications for the a priori assumption that all particle sizes have identical n_s values. This implies that kaolinite particles of different sizes feature similar ice nucleation properties. Note that this could only be achieved when accounting for multiply charged particles. An n_s parameterization (for T in degrees Celsius) can be given:

$$n_s(T) = \exp(-0.53T + 6.75). \tag{4}$$

Next, we consider the effect of multiply charged particles on the freezing probability. For that, the ice fractions of singly charged particles were calculated with

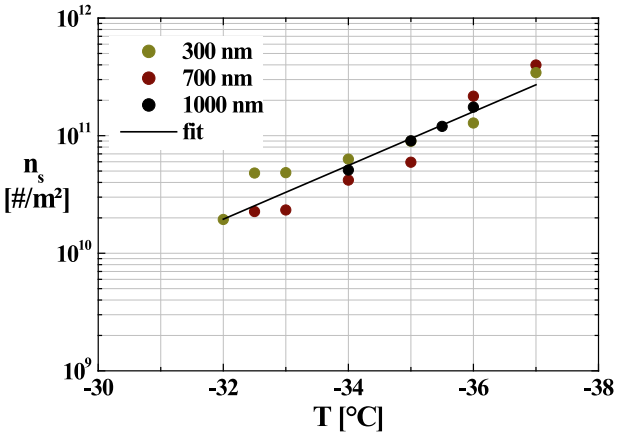

FIG. 5. Ice nucleation surface site density in dependence on temperature derived from different particle sizes by applying the correction for multiply charged particles.

Eq. (2) using the derived temperature-dependent ice surface site density and respective geometrical surface area for different particle sizes. In Fig. 4, the ice fractions of singly charged particles are illustrated by dots. For 700-nm particles, the charge correction leads to a slight shift of the ice fractions to lower values, but still in the range of the measurement uncertainties. However, the decrease of ice fractions when comparing uncorrected and multiply charge-corrected data is strongly pronounced for 300 nm, where the difference between the two datasets clearly exceeds the measurement uncertainty. This is not a surprising result as 300-nm kaolinite particles have a higher proportion of multiply charged particles than larger ones and the surface area increases quadratic with diameter, leading to much larger surface areas for multiply charged particles.

b. *Time-dependent description*

Ice nucleation is a time-dependent process by nature and we wanted to test how strong this time dependence is for the here-examined kaolinite sample and if we can reproduce it through modeling. We use a model based on classical nucleation theory (CNT), the so-called soccer ball model (SBM; Niedermeier et al. 2011a, 2014), to describe experimental results. For this, in the following, we first used the same measurements that had been introduced in the previous section (corrected for multiple charges) to derive a contact angle distribution. The contact angle distribution characterizes the freezing behavior of an ensemble of particles. The derivation is based on the presented LACIS measurements having a nucleation time of 1.6 s. We also used the so-determined contact angle distribution to model ice nucleation measurements obtained from literature (Welti et al. 2012), where a variety of nucleation times was applied, as will be shown later.

In the SBM, the surface of particles is thought to carry sites, where a specific contact angle θ is assigned to each of these surface sites. These sites will be called SBM sites in the following. The SBM allows for a variation of ice nucleation efficiencies of the different SBM sites; that is, it accounts for the heterogeneity of surface properties relevant for ice nucleation and particle-to-particle variations. In a macroscopic view, these ice nucleating sites can be considered as areas on the particles that provide inherently lower critical energy barriers compared to the remaining particle areas. Our understanding of the exact nature of these ice nucleating sites reducing the critical energy barrier is limited (Murray et al. 2012; Hoose and Möhler 2012; Zolles et al. 2015). However, evidence of beneficial properties of different nature was found that can lead to a reduction of the critical energy barrier. These might be, for example, a good lattice match with ice, the ability to interact with water molecules through electrostatic and hydrogen bonding, as well as cooperative mechanisms to achieve the lattice match with ice (Shen et al. 1977; Yakobi-Hancock et al. 2013; Zolles et al. 2015). In general, the ice nucleating sites are able to bind and arrange water molecules in a specific way and consequently act as template for the ice lattice. Following Zolles et al. (2015), these ice nucleating sites are not necessarily always similar, as they are formed, for example, by stochastically arranged functional groups able to bind water. In the present study, we follow the approach of a statistical distribution of ice nucleation efficiencies by using a contact angle distribution. The contact angle distribution is defined by a Gaussian probability density function $p(\theta)$ with mean value μ_θ and standard deviation σ_θ. For details, we refer to Niedermeier et al. (2014).

In addition, the surface area of each SBM site needs to be set, and a fixed value of $s_{\text{site}} = 10^{-14}\,\text{m}^2$ was selected. This value is the same as that used in Niedermeier et al. (2015), where it was chosen such that it is larger than the base area of the critical ice cluster and smaller than the surface area of the smallest mineral dust particle reported to induce freezing in Welti et al. (2014). All particles of the same size have the same number of sites n_{site}. Depending on the particle size, a different number of SBM sites is present on the particle surface, where n_{site} was assumed to scale with the total particle surface area. This assumption is strongly supported by findings from the time-independent approach (section 5a) and is in line with the concept of statistical distribution of ice nucleating sites, where, with increasing surface area, the probability for these ice nucleating sites is also increasing.

The probability of a single droplet to be unfrozen P_{unfr} at a given temperature T and time t can be expressed as

$$P_{\text{unfr}}(T,\mu_\theta,\sigma_\theta,t) = \int_0^{\pi} p(\theta)\exp[-j_{\text{het}}(T,\theta)s_{\text{site}}t]\,d\theta + \int_{-\infty}^{0} p(\theta)\exp[-j_{\text{het}}(T,\theta=0)s_{\text{site}}t]\,d\theta + \int_{\pi}^{\infty} p(\theta)\exp[-j_{\text{het}}(T,\theta=\pi)s_{\text{site}}t]\,d\theta \quad (5)$$

with the nucleation rate coefficient j_{het} [parameterizations according to Zobrist et al. (2007)].

The probability density function of a given contact angle is equal for each particle in the population. Consequently, the probability of freezing of a particle can be related to the ice fraction:

$$f_{\text{ice}}(T,\mu_\theta,\sigma_\theta,n_{\text{site}},t) = 1 - [P_{\text{unfr}}(T,\mu_\theta,\sigma_\theta,t)]^{n_{\text{site}}}. \quad (6)$$

Before applying the SBM to the data, the measured ice fractions were converted to an effective nucleation rate coefficient $j_{\text{het,eff}}$ in analogy to the determination of n_s. Equation (3) was used with $f_{\text{ice},i}(T) = 1 - \exp[-j_{\text{het,eff},i}(T)s_{p,i}t]$. All derived $j_{\text{het,eff}}$ fall together as expected; see Fig. 6.

Using the SBM, the best fit was obtained for n_{site} (300 nm) = 0.4, n_{site} (700 nm) = 2.2, and n_{site} (1000 nm) = 4.4 and the SBM parameters $\mu_\theta = 1.87$ rad and $\sigma_\theta = 0.25$ rad. The corresponding curve is shown in Fig. 6. The experimentally determined $j_{\text{het,eff}}$ and the SBM fit are well constrained within a factor of 2 as it was the case for n_s following the time-independent approach. The fact that a single SBM parameter set of μ_θ and σ_θ reproduces the experimental results is highly suggestive for the assumption made that the number of sites scales with particle surface area and hence the statement that kaolinite particles feature similar ice nucleation properties at different sizes, as it was already concluded from the time-independent description.

In addition to the SMB calculations based on a contact angle distribution, Fig. 6 also shows a curve that was obtained based on a single constant contact angle, only where the mean of the above given contact angle distribution was used. As already described in, for example, Zobrist et al. (2007), Hartmann et al. (2011), Rigg et al. (2013), and Augustin et al. (2013), a single constant contact angle is not capable of reproducing heterogeneous freezing results because the correct temperature dependence cannot be reproduced. Comparing the curves obtained when using a contact angle distribution and a single contact angle, it can be assumed that the ice nucleation sites on the examined kaolinite have heterogeneous ice nucleating properties; that is, the ice nucleation sites have different ice nucleation efficiency. This manifests in a comparably broad distribution of contact angles with $\sigma_\theta = 0.25$ rad. The best sites dominate the freezing behavior, which is seen in the fact that ice nucleation takes already place at higher temperatures than those predicted from the mean contact angle.

In the next step, the time dependence was examined. SBM calculations using different ice nucleation times were made. In Fig. 7, the ice fractions obtained in Welti et al. (2012) and the corresponding SBM parameterization are shown as a function of time for different temperatures. For the SBM parameterization, a larger number of sites were assumed than one would expect from the examined particle sizes as given in the paper. More precisely, instead of $n_{\text{site}} = 5.7$, which would correspond to 800-nm particles, $n_{\text{site}} = 32.4$ had to be used. This corresponds to a particle size of 1900 nm. Probably this effect is mainly caused by the neglect of multiply charged particles and hence by an underestimation of the particle surface area. A possible reason for this is discussed in section 6. However, the contact angle distribution derived from LACIS measurements ($\mu_\theta = 1.87$ rad and $\sigma_\theta = 0.25$ rad) can be applied to represent ice fractions given in Welti et al. (2012) as a function of temperature and time with reasonable confidence (root-mean-square error of 0.15), although largely differing ice nucleation/residence times were used to obtain these two datasets. This is an interesting result leading to the conclusion that the nature of ice nucleating sites seems to be very similar for the Fluka kaolinite investigated in both studies. Hence, both the study by Welti et al. (2012) and the here-presented analysis with the SBM show that a change in temperature of about 1 K corresponds to a change of one order of magnitude in ice nucleation time for the range investigated. As a result, from the present study, for the kaolinite investigated, a lowering of 1 K has the same effect as, for example, an increase in particle size from 500 to 700 nm or from 700 to 855 nm, assuming spherical particle shape.

Summarizing our conclusions from both time-independent and time-dependent descriptions of immersion freezing, (i) the kaolinite particles investigated have very similar ice nucleation properties at different particle sizes. This is a necessary condition to derive, for example, (ii) the same temperature-dependent ice nucleation surface site density or alternatively the same contact angle distribution for different particle sizes. Consequently, (iii) the probability of freezing

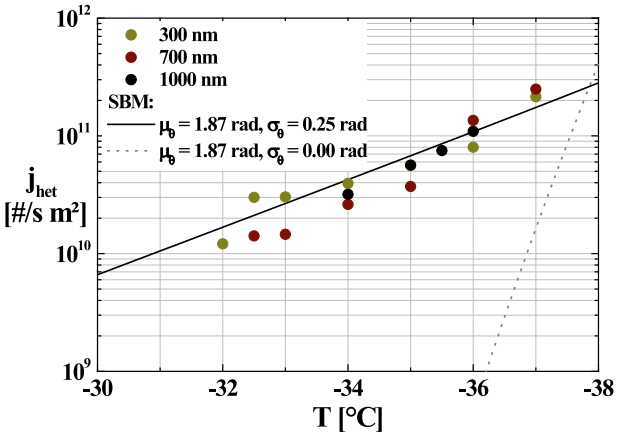

FIG. 6. Comparison of experimentally determined effective nucleation rate coefficient accounting for multiple charge correction and respective SBM fit (black line) accounting for a contact angle distribution at different temperatures. The same color code is used as before. Additionally, a curve for a single constant contact angle ($\theta = 1.87$ rad; gray dotted line) is given.

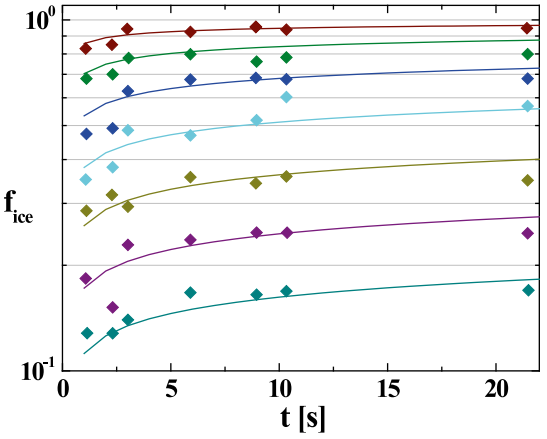

FIG. 7. Comparison of experimental [800-nm kaolinite particles from Welti et al. (2012); symbols] and SBM fit results (lines) for ice fractions as a function of time at different temperatures (top down: from −36° to −30°C in 1-K steps). Note that the whole dataset of Welti et al. (2012) and the present study could be reproduced with a single parameter set of the SBM: $\mu_\theta = 1.87$ rad and $\sigma_\theta = 0.25$ rad.

scales exponentially with particle surface area ($f_{ice} \propto e^{s_p}$). To our knowledge, the scaling of the freezing probability with particle surface area in the immersion mode was documented for the first time for monodisperse particles where only one particle is immersed in each droplet.

6. Discussion

In the literature, there are a number of studies investigating the immersion freezing capability of mineral dust in particular kaolinite. Kaolinite samples from different sources vary concerning physical and chemical properties (Murray et al. 2011; Pinti et al. 2012; Wex et al. 2014). Therefore, for comparison, we choose the studies of Lüönd et al. (2010) and Welti et al. (2012) in which kaolinite from the same provider (Fluka; same as that from Sigma-Aldrich) was used. In both studies the same instrument, a combination of Immersion Mode Cooling Chamber–Zurich Ice Nucleation Chamber (IMCA–ZINC; Lüönd et al. 2010), was applied for the measurements. To study the immersion freezing results of the three studies, we compare the ice nucleation surface site densities since it was used for this purpose in the literature (e.g., Murray et al. 2012) and was applied as model input parameter for describing heterogeneous ice nucleation (e.g., Paukert and Hoose 2014). The comparison of n_s values helps to study the comparability of different instruments and the impact of time on the immersion freezing ability.

Beginning with results obtained in the present study, n_s for the multiply charge-corrected 300-, 700-, and 1000-nm kaolinite particles fall together (fit, black line) as already shown in Fig. 5 and again now in Fig. 8. The scatter of values is less than a factor of 3 from the lowest to the largest value at any temperature.

Considering the n_s values determined from the study of Lüönd et al. (2010) and Welti et al. (2012), data points obtained for residence times of 9 and 14 s shown in Fig. 8 can be presented together (fit, brown line) although they scatter a little more than half an order of magnitude. The comparison of results from these two earlier studies and the present study clearly demonstrates an offset in derived n_s values of roughly an order of magnitude. As n_s is assumed to be an instrument-independent quantity, and as similar particles from the same kaolinite source were analyzed using a comparable method, this discrepancy is unexpectedly high and needs to be discussed. Potential reasons for this discrepancy in the absolute values of n_s could be effects of (i) differences concerning chemical and physical properties in the kaolinite sample, (ii) ice nucleation time, and (iii) an underestimated surface area due to the neglect of multiply charged particles (i.e., differences in the expected particle surface area).

Kaolinite purchased from Fluka is an industrial product. Differences in different Fluka kaolinite samples (from batch to batch) might affect the efficiency of freezing concerning (i). However, looking at Fig. 8, it can be seen that we found a similar temperature

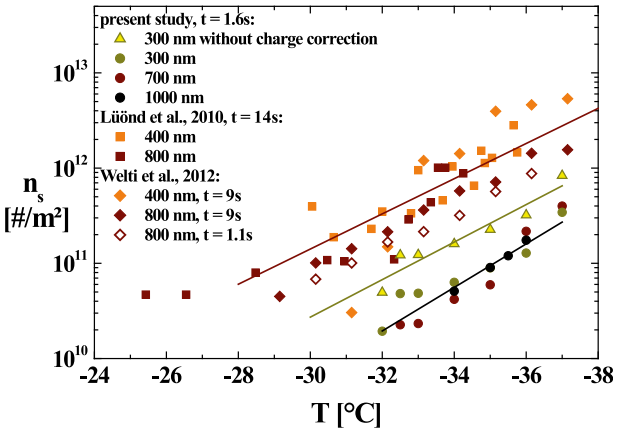

FIG. 8. The ice nucleation surface site density is given as a function of temperature. Results are shown from Fluka kaolinite gained in the studies of Lüönd et al. (2010), Welti et al. (2012), and the present study. All n_s values derived from ice fractions given in Lüönd et al. (2010) and Welti et al. (2012) for measurements with residence times of 14 and 9 s are averaged for clarity, represented by a fit (brown line). The LACIS data for all charge-corrected and for the uncorrected 300-nm particles are summarized by the black and dark yellow lines, respectively.

dependence (i.e., a similar slope) of the ice nucleation behavior for our data and the data from Welti et al. (2012) and Lüönd et al. (2010). This, as well as the fact that the datasets could be described with the same contact angle distribution, indicates a similar type of ice activity. However, it has been discussed in the literature that the K-feldspar content in the kaolinite determines the ice activity of the samples (Atkinson et al. 2013; Augustin-Bauditz et al. 2014). The detection of the fraction of K-feldspar in a mineral dust sample is demanding, and this fraction depends on the degree of weathering in a sample (Wex et al. 2014; Augustin-Bauditz et al. 2014). It can therefore not be dismissed that this fraction might vary between different Fluka kaolinite samples. However, this is difficult to prove and speculative at the current stage. But we want to state explicitly that such a difference in the fraction of K-feldspar between two samples would lead to, for example, different n_s values but the temperature dependence in the observed freezing behavior would be unaffected.

Following the concept of the ice nucleation surface site density, the time dependence of freezing is completely neglected. The compared measurements were carried out for different ice nucleation times. Concerning (ii), this could contribute to the observed offset in n_s. In Wex et al. (2014) it was found that results from CFDC (DeMott et al. 2010) and LACIS using identical seed particles for their ice nucleation experiments coincide when accounting for the respective residence times in the instruments (5 and 1.6 s for the CFDC and LACIS, respectively). This agreement was slightly diminished when a time-independent approach was used. This could also be the case here, particularly as most data obtained by Lüönd et al. (2010) and Welti et al. (2012) were taken for residence times of 14 and 9 s, respectively. Only one dataset from Welti et al. (2012) for 800 nm was taken for $t_{ice} = 1.1$ s (open brown diamonds in Fig. 8). This residence time is close to the LACIS ice nucleation time, but still the respective n_s values are above those that we obtained in this study. On the other hand, these n_s values from Welti et al. (2012) are clearly lower than all other n_s values derived from Lüönd et al. (2010) and Welti et al. (2012) for the longer residence times, by roughly a factor of 2. This is rooted in the above described effect, that an increase in residence time by one order of magnitude corresponds to an increase of the observed freezing by 1 K. While this explains some of the scatter in the data from Lüönd et al. (2010) and Welti et al. (2012) and somewhat diminishes the deviation between data from these two studies and from LACIS, some of the discrepancy still remains. Values of n_s for 1.1 s from Welti et al. (2012) are a factor of 2 above data from LACIS for 300 nm, which were not corrected for multiple charges, while they deviate much more from charge-corrected data. This is discussed in the following section.

Concerning (iii), the neglect of a possible underestimation of the surface area due to multiply charged particles in the aerosol could lead to an overestimation of the ice nucleation surface site density. In the following, we indicate how large the overestimation of n_s due to neglected multiply charged particles can be. In Fig. 8 the n_s values derived from uncorrected 300-nm kaolinite particles from the present study and the corresponding fit are presented. The n_s values are higher than those which have been corrected for multiply charged particles, shifting the observed freezing curve by roughly 2 K. Instead of a temperature shift of around 5 K that was originally observed between LACIS and Lüönd et al. (2010) and Welti et al. (2012), the temperature difference between data from Welti et al. (2012) taken for a residence time of 1.1 s and the uncorrected LACIS data is only around 1–2 K. This strongly supports that the observed discrepancy of the absolute n_s values mostly results from a neglect of the contribution of multiply charged particles to the total particle surface area. In our study, we used a preimpactor and still observed a significant fraction of unexpected multiply charged particles. If no or an inefficient preimpaction system is used, then the amount of multiply charged particles in

the aerosol sample might be even higher, particularly for the examined kaolinite sample.

In section 5b, a higher surface area corresponding to an effective particle size of 1900 nm in diameter needed to be assumed in order to model data given in Welti et al. (2012) at different times with the SBM. Concluding from the discussion above, the particles could, for example, be made up of equal fractions of singly, doubly, triply, and fourthfold charged 800-nm particles to result in an effective particle size of 1900 nm. However, this is a theoretical exercise and without the measurement of the number size distribution of the size-selected particles, which strongly depends on the exact setup of the particle generation, there is no possibility to judge how realistic this is.

Studying the immersion freezing behavior of another mineral dust (ATD) using the same particle generation method, in Niedermeier et al. (2010) and Niedermeier et al. (2011b), it was found that multiply charged particles played a negligible role. So during aerosol generation, the occurrence of multiply charged particles strongly depends on the properties of the sample and on the generation method. The Fluka kaolinite particles appear to be particularly prone to collect multiple charges because the same particle generation was used in Niedermeier et al. (2010), Niedermeier et al. (2011b), and in the present study, and the fractions of multiply charged kaolinite particles were clearly higher than those observed for ATD. That clearly shows how important it is to determine the fraction of multiply charged particles when investigating quasi-monodisperse particles generated with a DMA.

Altogether, the observed discrepancy of the ice nucleation surface site density results maybe from differences in the fractions of the K-feldspar content (an effect difficult to quantify), from differences in the ice nucleation time, and most likely to the largest extent from an underestimated particle surface area due to the neglect of multiply charged particles. When applying the SBM and allowing for a difference in the surface area alone, which corresponds to assuming a higher number of SBM sites than one would have expected (section 5b), we observed the same temporal behavior of immersion freezing as it was found in Welti et al. (2012).

7. Summary and conclusions

The immersion freezing capability of quasi-monodisperse size-selected kaolinite particles was investigated as a function of temperature and particle size at a known ice nucleation time. Kaolinite particles of 300-, 700-, and 1000-nm mobility diameter were selected with a DMA. Utilizing the laminar flow tube LACIS, in separate experiments these quasi-monodisperse kaolinite particles were activated to cloud droplets and some droplets froze, as a consequence of cooling. The ice fractions were measured in a temperature range from −30°C down to the homogeneous freezing limit.

To study the scaling of the freezing probability with particle surface area in the immersion freezing mode, as a necessary condition, we first demonstrated that immersion freezing does not depend on droplet volume. Further, we found multiply charged particles occurring in the quasi-monodisperse kaolinite aerosol. From droplet activation measurements conducted with a CCN counter, we were able to determine the fractions of multiply charged particles at different sizes. An unexpectedly high amount of multiply charged particles was found even though a preimpaction system was applied upstream of the DMA. Multiply charged particles are larger and hence have higher surface areas than singly charged particles, which significantly influences the ice nucleation probability. As a consequence, a multiple charge correction method was developed in order to correct measured ice fraction and derive quantities for singly charged particles. In particular, for the 300-nm kaolinite particles, the comparison of uncorrected and corrected ice fractions shows that the observed difference significantly exceeds the measurement uncertainty.

Analyzing the ice fraction as a function of temperature, we found that the ice fraction increases exponentially with temperature and that the ice fractions measured for different kaolinite particle sizes show a similar temperature dependence. From that, we can conclude that differently sized kaolinite particles feature similar ice nucleation properties. Based on the multiple charge correction method, we could show the dependence of immersion freezing on particle surface area. In other words, the probability of freezing scales exponentially with particle surface area. To our knowledge, this is shown for the first time for monodisperse particles where only one INP is immersed in each droplet. Data for differently sized particles at a fixed ice nucleation time could be described consistently by both theoretical approaches available in the literature: a time-independent approach (n_s-type parameterization) and a time-dependent approach (based on classical nucleation theory, including a contact angle distribution). Therefore, both the time-independent and time-dependent descriptions corroborate that the kaolinite particles investigated at LACIS have identical ice nucleation properties at different particle sizes. Moreover, using the contact

angle distribution, the ice nucleating ability of kaolinite investigated in Welti et al. (2012) could be modeled for different ice nucleation times assuming a higher number of sites being present as expected.

Further, the comparison of the present study with Lüönd et al. (2010) and Welti et al. (2012) using kaolinite from the same provider and a comparable experimental method shows that temperature dependence of the ice nucleation surface site density is similar in all three studies, again suggesting that kaolinite with very similar ice nucleation properties was examined. However, we observed a significant offset between the derived n_s values of about one order of magnitude or a temperature shift of around 5–6 K, which we assume to originate mostly in the neglect of multiply charged particles and hence in an underestimated surface area in both Lüönd et al. (2010) and Welti et al. (2012) and, to a lesser extent, in a small effect of time. This clearly indicates how important it is to account for the fraction of multiply charged particles when using the DMA for size selection.

Acknowledgments. S.H. acknowledges personal funding by a scholarship program by SMWK. H.W. thanks funding by DFG within the research unit FOR 1525 INUIT (4722/1-1). D.N. acknowledges financial support from the Alexander von Humboldt Foundation.

APPENDIX

Freezing Probability of Externally Mixed INPs

We consider a droplet ensemble of N_0 droplets. Each droplet contains one particle, where, for the study presented here, the particles have different sizes, being singly, doubly, and triply charged particles of the same electric mobility diameter. It should be mentioned that the same treatment can also be done for ensembles of INPs, which consist of external mixtures of, for example, different substances. The total number of droplets is defined as sum of the number of droplets belonging to ith subpopulation, where each subpopulation contains particles of a single size or at least a narrow size range. It can be written as the sum of the number of droplets of the respective subpopulations $N_{0,i}$ or, alternatively, as the sum of products of fraction of occurrence a_i (with $\sum_{i=0}^{n} a_i = 1$) and N_0:

$$N_0 = \sum_{i=0}^{n} N_{0,i} = \sum_{i=0}^{n} a_i N_0 . \tag{A1}$$

Similarly, the total number of unfrozen droplets N_u can be calculated by

$$N_u = \sum_{i=0}^{n} N_{u,i} = \sum_{i=0}^{n} a_i N_u . \tag{A2}$$

The total unfrozen fraction can be expressed as

$$\frac{N_u}{N_0} = \frac{1}{N_0} \sum_{i=0}^{n} N_{u,i} = \sum_{i=0}^{n} \frac{N_{u,i}}{N_0} . \tag{A3}$$

For the next step, the singular approach is applied to describe the freezing behavior [Eq. (2)]. The ice nucleation surface site density of the subpopulation i can be expressed as $n_{s,i}$. Then it follows that

$$\frac{N_{u,i}(T)}{N_0} = \exp[-n_{s,i}(T) s_{p,i}] \tag{A4}$$

with the surface area $s_{p,i}$ of particle type i. Then the total unfrozen fraction of the external mixture can be written as

$$\frac{N_u(T)}{N_0} = \sum_{i=0}^{n} a_i \exp[-n_{s,i}(T) s_{p,i}] . \tag{A5}$$

Equation (A5) corresponds to the superposition of the unfrozen fractions weighted by the fraction of subpopulation type i. The same holds for the ice fraction f_{ice} of the externally mixed droplet ensemble. Using $N_u/N_0 = 1 - f_{\mathrm{ice}}$ and $f_{\mathrm{ice},i} = 1 - \exp[-n_{s,i}(T) s_{p,i}]$ it follows that

$$f_{\mathrm{ice}}(T) = \sum_{i=1}^{n} a_i f_{\mathrm{ice},i}(T) . \tag{A6}$$

As a result, the ice fraction of the externally mixed droplet ensemble can be calculated by the superposition of the ice fractions of subpopulation i weighted by their fraction of occurrence. Equation (A6) can also be valid for other theoretical concepts instead of the ice nucleation surface site density.

REFERENCES

Alpert, P. A., J. Y. Aller, and D. A. Knopf, 2011: Ice nucleation from aqueous NACL droplets with and without marine diatoms. *Atmos. Chem. Phys.*, **11**, 5539–5555, doi:10.5194/acp-11-5539-2011.

Ansmann, A., and Coauthors, 2009: Evolution of the ice phase in tropical altocumulus: SAMUM lidar observations over Cape Verde. *J. Geophys. Res.*, **114**, D17208, doi:10.1029/2008jd011659.

Archuleta, C. M., P. J. DeMott, and S. M. Kreidenweis, 2005: Ice nucleation by surrogates for atmospheric mineral dust and mineral dust/sulfate particles at cirrus temperatures. *Atmos. Chem. Phys.*, **5**, 2617–2634, doi:10.5194/acp-5-2617-2005.

Arnold, E., J. Merrill, M. Leinen, and J. King, 1998: The effect of source area and atmospheric transport on mineral aerosol collected over the North Pacific Ocean. *Global Planet. Change*, **18**, 137–159, doi:10.1016/S0921-8181(98)00013-7.

Atkinson, J. D., and Coauthors, 2013: The importance of feldspar for ice nucleation by mineral dust in mixed-phase clouds. *Nature*, **498**, 355–358, doi:10.1038/nature12278.

Augustin, S., and Coauthors, 2013: Immersion freezing of birch pollen washing water. *Atmos. Chem. Phys.*, **13**, 10 989–11 003, doi:10.5194/acp-13-10989-2013.

Augustin-Bauditz, S., H. Wex, S. Kanter, M. Ebert, D. Niedermeier, F. Stolz, A. Prager, and F. Stratmann, 2014: The immersion mode ice nucleation behavior of mineral dusts: A comparison of different pure and surface modified dusts. *Geophys. Res. Lett.*, **41**, 7375–7382, doi:10.1002/2014GL061317.

Avila, A., I. Queralt-Mitjans, and M. Alarcon, 1997: Mineralogical composition of African dust delivered by red rains over northeastern Spain. *J. Geophys. Res.*, **102**, 21 977–21 996, doi:10.1029/97JD00485.

Bigg, E. K., 1953: The formation of atmospheric ice crystals by the freezing of droplets. *Quart. J. Roy. Meteor. Soc.*, **79**, 510–519, doi:10.1002/qj.49707934207.

Blanco, A., F. De Tomasi, E. Filippo, D. Manno, M. R. Perrone, A. Serra, A. M. Tafuro, and A. Tepore, 2003: Characterization of African dust over southern Italy. *Atmos. Chem. Phys.*, **3**, 2147–2159, doi:10.5194/acp-3-2147-2003.

Broadley, S. L., B. J. Murray, R. J. Herbert, J. D. Atkinson, S. Dobbie, T. L. Malkin, E. Condliffe, and L. Neve, 2012: Immersion mode heterogeneous ice nucleation by an illite rich powder representative of atmospheric mineral dust. *Atmos. Chem. Phys.*, **12**, 287–307, doi:10.5194/acp-12-287-2012.

Chester, R., E. J. Sharples, G. S. Sanders, and A. C. Saydam, 1984: Saharan dust incursion over the Tyrrhenian Sea. *Atmos. Environ.*, **18**, 929–935, doi:10.1016/0004-6981(84)90069-6.

Clauss, T., A. Kiselev, S. Hartmann, S. Augustin, S. Pfeifer, D. Niedermeier, H. Wex, and F. Stratmann, 2013: Application of linear polarized light for the discrimination of frozen and liquid droplets in ice nucleation experiments. *Atmos. Meas. Tech.*, **6**, 1041–1052, doi:10.5194/amt-6-1041-2013.

Connolly, P. J., O. Moehler, P. R. Field, H. Saathoff, R. Burgess, T. Choularton, and M. Gallagher, 2009: Studies of heterogeneous freezing by three different desert dust samples. *Atmos. Chem. Phys.*, **9**, 2805–2824, doi:10.5194/acp-9-2805-2009.

de Boer, G., H. Morrison, M. D. Shupe, and R. Hildner, 2011: Evidence of liquid dependent ice nucleation in high-latitude stratiform clouds from surface remote sensors. *Geophys. Res. Lett.*, **38**, L01803, doi:10.1029/2010GL046016.

DeMott, P. J., D. J. Cziczo, A. J. Prenni, D. M. Murphy, S. M. Kreidenweis, D. S. Thomson, R. Borys, and D. C. Rogers, 2003a: Measurements of the concentration and composition of nuclei for cirrus formation. *Proc. Natl. Acad. Sci. USA*, **100**, 14 655–14 660, doi:10.1073/pnas.2532677100.

——, K. Sassen, M. R. Poellot, D. Baumgardner, D. C. Rogers, S. D. Brooks, A. J. Prenni, and S. M. Kreidenweis, 2003b: African dust aerosols as atmospheric ice nuclei. *Geophys. Res. Lett.*, **30**, 1732, doi:10.1029/2003gl017410.

——, and Coauthors, 2010: Predicting global atmospheric ice nuclei distributions and their impacts on climate. *Proc. Natl. Acad. Sci. USA*, **107**, 11 217–11 222, doi:10.1073/pnas.0910818107.

Diehl, K., and S. K. Mitra, 1998: A laboratory study of the effects of a kerosene-burner exhaust on ice nucleation and the evaporation rate of ice crystals. *Atmos. Environ.*, **32**, 3145–3151, doi:10.1016/S1352-2310(97)00467-6.

——, and S. Wurzler, 2004: Heterogeneous drop freezing in the immersion mode: Model calculations considering soluble and insoluble particles in the drops. *J. Atmos. Sci.*, **61**, 2063–2072, doi:10.1175/1520-0469(2004)061<2063:HDFITI>2.0.CO;2.

——, S. Matthias-Maser, R. Jaenicke, and S. K. Mitra, 2002: The ice nucleating ability of pollen: Part II. Laboratory studies in immersion and contact freezing modes. *Atmos. Res.*, **61**, 125–133, doi:10.1016/S0169-8095(01)00132-6.

——, M. Simmel, and S. Wurzler, 2006: Numerical sensitivity studies on the impact of aerosol properties and drop freezing modes on the glaciation, microphysics, and dynamics of clouds. *J. Geophys. Res.*, **111**, D07202, doi:10.1029/2005JD005884.

Ganor, E., 1991: The composition of clay minerals transported to Israel as indicators of Saharan dust emission. *Atmos. Environ.*, **25A**, 2657–2664, doi:10.1016/0960-1686(91)90195-d.

——, and Y. Mamane, 1982: Transport of Saharan dust across the eastern Mediterranean. *Atmos. Environ.*, **16**, 581–587, doi:10.1016/0004-6981(82)90167-6.

Glaccum, R. A., and J. M. Prospero, 1980: Saharan aerosols over the tropical North Atlantic—Mineralogy. *Mar. Geol.*, **37**, 295–321, doi:10.1016/0025-3227(80)90107-3.

Hartmann, S., D. Niedermeier, J. Voigtlaender, T. Clauss, R. A. Shaw, H. Wex, A. Kiselev, and F. Stratmann, 2011: Homogeneous and heterogeneous ice nucleation at LACIS: Operating principle and theoretical studies. *Atmos. Chem. Phys.*, **11**, 1753–1767, doi:10.5194/acp-11-1753-2011.

Hiranuma, N., and Coauthors, 2015: A comprehensive laboratory study on the immersion freezing behavior of illite NX particles: A comparison of 17 ice nucleation measurement techniques. *Atmos. Chem. Phys.*, **15**, 2489–2518, doi:10.5194/acp-15-2489-2015.

Hoffer, T. E., 1961: A laboratory investigation of droplet freezing. *J. Meteor.*, **18**, 766–778, doi:10.1175/1520-0469(1961)018<0766:ALIODF>2.0.CO;2.

Hoose, C., and O. Möhler, 2012: Heterogeneous ice nucleation on atmospheric aerosols: A review of results from laboratory experiments. *Atmos. Chem. Phys.*, **12**, 9817–9854, doi:10.5194/acp-12-9817-2012.

Johnson, L. R., 1976: Particle-size fractionation of eolian dusts during transport and sampling. *Mar. Geol.*, **21**, M17–M21, doi:10.1016/0025-3227(76)90099-2.

Kaaden, N., and Coauthors, 2009: State of mixing, shape factor, number size distribution, and hygroscopic growth of the Saharan anthropogenic and mineral dust aerosol at Tinfou, Morocco. *Tellus*, **61B**, 51–63, doi:10.1111/j.1600-0889.2008.00388.x.

Kamphus, M., and Coauthors, 2010: Chemical composition of ambient aerosol, ice residues and cloud droplet residues in mixed-phase clouds: Single particle analysis during the Cloud and Aerosol Characterization Experiment (CLACE 6). *Atmos. Chem. Phys.*, **10**, 8077–8095, doi:10.5194/acp-10-8077-2010.

Kandler, K., and Coauthors, 2007: Chemical composition and complex refractive index of Saharan mineral dust at Izana, Tenerife (Spain) derived by electron microscopy. *Atmos. Environ.*, **41**, 8058–8074, doi:10.1016/j.atmosenv.2007.06.047.

——, and Coauthors, 2009: Size distribution, mass concentration, chemical and mineralogical composition and derived optical parameters of the boundary layer aerosol at Tinfou, Morocco,

during SAMUM 2006. *Tellus*, **61B**, 32–50, doi:10.1111/j.1600-0889.2008.00385.x.

——, and Coauthors, 2011: Electron microscopy of particles collected at Praia, Cape Verde, during the Saharan mineral dust experiment: Particle chemistry, shape, mixing state and complex refractive index. *Tellus*, **63B**, 475–496, doi:10.1111/j.1600-0889.2011.00550.x.

Knopf, D. A., and P. A. Alpert, 2013: A water activity based model of heterogeneous ice nucleation kinetics for freezing of water and aqueous solution droplets. *Faraday Discuss.*, **165**, 513–534, doi:10.1039/c3fd00035d.

Knutson, E. O., and K. T. Whitby, 1975: Aerosol classification by electric mobility: Apparatus, theory, and applications. *J. Aerosol Sci.*, **6**, 443–451, doi:10.1016/0021-8502(75)90060-9.

Kumai, M., 1961: Snow crystals and the identification of the nuclei in the northern United States of America. *J. Meteor.*, **18**, 139–150, doi:10.1175/1520-0469(1961)018<0139:SCATIO>2.0.CO;2.

Langham, E. J., and B. J. Mason, 1958: The heterogeneous and homogeneous nucleation of supercooled water. *Proc. Roy. Soc. London*, **247A**, 493–504, doi:10.1098/rspa.1958.0207.

Leinert, S., 2002: Hygroscopicity of micrometer-sized aerosol particles—A new measurement technique. Ph.D. dissertation, University of Leipzig, 137 pp.

Levin, J., 1950: Statistical explanation of spontaneous freezing of water droplet. National Advisory Committee for Aeronautics Tech. Note 2234, 28 pp. [Available online at http://ntrs.nasa.gov/archive/nasa/casi.ntrs.nasa.gov/19930082877.pdf.]

Lohmann, U., 2006: Aerosol effects on clouds and climate. *Space Sci. Rev.*, **125**, 129–137, doi:10.1007/s11214-006-9051-8.

Lüönd, F., O. Stetzer, A. Welti, and U. Lohmann, 2010: Experimental study on the ice nucleation ability of size-selected kaolinite particles in the immersion mode. *J. Geophys. Res.*, **115**, D14201, doi:10.1029/2009JD012959.

Mahowald, N. M., and C. Luo, 2003: A less dusty future? *Geophys. Res. Lett.*, **30**, 1903, doi:10.1029/2003gl017880.

Marcolli, C., S. Gedamke, T. Peter, and B. Zobrist, 2007: Efficiency of immersion mode ice nucleation on surrogates of mineral dust. *Atmos. Chem. Phys.*, **7**, 5081–5091, doi:10.5194/acp-7-5081-2007.

Maring, H., D. L. Savoie, M. A. Izaguirre, L. Custals, and J. S. Reid, 2003: Mineral dust aerosol size distribution change during atmospheric transport. *J. Geophys. Res.*, **108**, 8592, doi:10.1029/2002JD002536.

Mason, B. J., 1960: Ice-nucleating properties of clay minerals and stony meteorites. *Quart. J. Roy. Meteor. Soc.*, **86**, 552–556, doi:10.1002/qj.49708637014.

——, and J. Maybank, 1958: Ice-nucleating properties of some natural mineral dusts. *Quart. J. Roy. Meteor. Soc.*, **84**, 235–241, doi:10.1002/qj.49708436104.

Mertes, S., and Coauthors, 2007: Counterflow virtual impact or based collection of small ice particles in mixed-phase clouds for the physico-chemical characterization of tropospheric ice nuclei: Sampler description and first case study. *Aerosol Sci. Technol.*, **41**, 848–864, doi:10.1080/02786820701501881.

Murray, B. J., S. L. Broadley, T. W. Wilson, J. D. Atkinson, and R. H. Wills, 2011: Heterogeneous freezing of water droplets containing kaolinite particles. *Atmos. Chem. Phys.*, **11**, 4191–4207, doi:10.5194/acp-11-4191-2011.

——, D. O'Sullivan, J. D. Atkinson, and M. E. Webb, 2012: Ice nucleation by particles immersed in supercooled cloud droplets. *Chem. Soc. Rev.*, **41**, 6519–6554, doi:10.1039/c2cs35200a.

Niedermeier, D., and Coauthors, 2010: Heterogeneous freezing of droplets with immersed mineral dust particles—Measurements and parameterization. *Atmos. Chem. Phys.*, **10**, 3601–3614, doi:10.5194/acp-10-3601-2010.

——, R. A. Shaw, S. Hartmann, H. Wex, T. Clauss, J. Voigtlaender, and F. Stratmann, 2011a: Heterogeneous ice nucleation: Exploring the transition from stochastic to singular freezing behavior. *Atmos. Chem. Phys.*, **11**, 8767–8775, doi:10.5194/acp-11-8767-2011.

——, and Coauthors, 2011b: Experimental study of the role of physicochemical surface processing on the IN ability of mineral dust particles. *Atmos. Chem. Phys.*, **11**, 11 131–11 144, doi:10.5194/acp-11-11131-2011.

——, B. Ervens, T. Clauss, J. Voigtlaender, H. Wex, S. Hartmann, and F. Stratmann, 2014: A computationally efficient description of heterogeneous freezing: A simplified version of the soccer ball model. *Geophys. Res. Lett.*, **41**, 736–741, doi:10.1002/2013GL058684.

——, S. Augustin-Bauditz, S. Hartmann, H. Wex, K. Ignatius, and F. Stratmann, 2015: Can we define an asymptotic value for the ice active surface site density for heterogeneous ice nucleation? *J. Geophys. Res. Atmos.*, **120**, 5036–5046, doi:10.1002/2014JD022814.

Niemand, M., and Coauthors, 2012: A particle-surface-area-based parameterization of immersion freezing on desert dust particles. *J. Atmos. Sci.*, **69**, 3077–3092, doi:10.1175/JAS-D-11-0249.1.

Paukert, M., and C. Hoose, 2014: Modeling immersion freezing with aerosol-dependent prognostic ice nuclei in Arctic mixed-phase clouds. *J. Geophys. Res. Atmos.*, **119**, 9073–9092, doi:10.1002/2014JD021917.

Pinti, V., C. Marcolli, B. Zobrist, C. R. Hoyle, and T. Peter, 2012: Ice nucleation efficiency of clay minerals in the immersion mode. *Atmos. Chem. Phys.*, **12**, 5859–5878, doi:10.5194/acp-12-5859-2012.

Pitter, R. L., and H. R. Pruppacher, 1973: Wind-tunnel investigation of freezing of small water drops falling at terminal velocity in air. *Quart. J. Roy. Meteor. Soc.*, **99**, 540–550, doi:10.1002/qj.49709942111.

Pratt, K. A., and Coauthors, 2009: In situ detection of biological particles in cloud ice-crystals. *Nat. Geosci.*, **2**, 398–401, doi:10.1038/ngeo521.

Pruppacher, H. R., and J. D. Klett, 1997: *Microphysics of Clouds and Precipitation.* Kluwer Academic Publishers, 954 pp.

Raddatz, M., A. Wiedensohler, H. Wex, and F. Stratmann, 2013: Size selection of sub- and super-micron clay mineral kaolinite particles using a custom-built maxi-DMA. *Proc. 19th Int. Conf. on Nucleation and Atmospheric Aerosols*, Fort Collins, CO, American Institute of Physics, 457–460.

Richardson, M. S., and Coauthors, 2007: Measurements of heterogeneous ice nuclei in the western United States in springtime and their relation to aerosol characteristics. *J. Geophys. Res.*, **112**, D02209, doi:10.1029/2006JD007500.

Rigg, Y. J., P. A. Alpert, and D. A. Knopf, 2013: Immersion freezing of water and aqueous ammonium sulfate droplets initiated by humic-like substances as a function of water activity. *Atmos. Chem. Phys.*, **13**, 6603–6622, doi:10.5194/acp-13-6603-2013.

Roberts, G. C., and A. Nenes, 2005: A continuous-flow streamwise thermal-gradient CCN chamber for atmospheric measurements. *Aerosol Sci. Technol.*, **39**, 206–221, doi:10.1080/027868290913988.

Sassen, K., P. J. DeMott, J. M. Prospero, and M. R. Poellot, 2003: Saharan dust storms and indirect aerosol effects on clouds: CRYSTAL-FACE results. *Geophys. Res. Lett.*, **30**, 1633, doi:10.1029/2003gl017371.

Seifert, P., and Coauthors, 2010: Saharan dust and heterogeneous ice formation: Eleven years of cloud observations at a central European EARLINET site. *J. Geophys. Res.*, **115**, D20201, doi:10.1029/2009JD013222.

Shen, J. H., K. Klier, and A. C. Zettlemoyer, 1977: Ice nucleation by micas. *J. Atmos. Sci.*, **34**, 957–960, doi:10.1175/1520-0469(1977)034<0957:INBM>2.0.CO;2.

Stratmann, F., and Coauthors, 2004: Laboratory studies and numerical simulations of cloud droplet formation under realistic supersaturation conditions. *J. Atmos. Oceanic Technol.*, **21**, 876–887, doi:10.1175/1520-0426(2004)021<0876:LSANSO>2.0.CO;2.

Sullivan, R., and Coauthors, 2010: Irreversible loss of ice nucleation active sites in mineral dust particles caused by sulphuric acid condensation. *Atmos. Chem. Phys.*, **10**, 11 471–11 487, doi:10.5194/acp-10-11471-2010.

Twohy, C. H., and M. R. Poellot, 2005: Chemical characteristics of ice residual nuclei in anvil cirrus clouds: Evidence for homogeneous and heterogeneous ice formation. *Atmos. Chem. Phys.*, **5**, 2289–2297, doi:10.5194/acp-5-2289-2005.

Welti, A., F. Lueoend, O. Stetzer, and U. Lohmann, 2009: Influence of particle size on the ice nucleating ability of mineral dusts. *Atmos. Chem. Phys.*, **9**, 6705–6715, doi:10.5194/acp-9-6705-2009.

——, ——, Z. A. Kanji, O. Stetzer, and U. Lohmann, 2012: Time dependence of immersion freezing: An experimental study on size selected kaolinite particles. *Atmos. Chem. Phys.*, **12**, 9893–9907, doi:10.5194/acp-12-9893-2012.

——, U. Lohmann, and Z. A. Kanji, 2014: Is there a lower size limit for mineral dust ice nuclei in the immersion mode? *Geophysical Research Abstracts*, Vol. 16, Abstract EGU2014-6722. [Available online at http://meetingorganizer.copernicus.org/EGU2014/EGU2014-6722.pdf.]

Westbrook, C. D., and A. J. Illingworth, 2011: Evidence that ice forms primarily in supercooled liquid clouds at temperatures > −27°C. *Geophys. Res. Lett.*, **38**, L14808, doi:10.1029/2011GL048021.

Wex, H., and Coauthors, 2014: Kaolinite particles as ice nuclei: Learning from the use of different kaolinite samples and different coatings. *Atmos. Chem. Phys.*, **14**, 5529–5546, doi:10.5194/acp-14-5529-2014.

Yakobi-Hancock, J. D., L. A. Ladino, and J. P. D. Abbatt, 2013: Feldspar minerals as efficient deposition ice nuclei. *Atmos. Chem. Phys.*, **13**, 11 175–11 185, doi:10.5194/acp-13-11175-2013.

Zobrist, B., T. Koop, B. P. Luo, C. Marcolli, and T. Peter, 2007: Heterogeneous ice nucleation rate coefficient of water droplets coated by a nonadecanol monolayer. *J. Phys. Chem.*, **111C**, 2149–2155, doi:10.1021/jp066080w.

Zolles, T., J. Burkart, T. Haeusler, B. Pummer, R. Hitzenberger, and H. Grothe, 2015: Identification of ice nucleation active sites on feldspar dust particles. *J. Phys. Chem.*, **119A**, 2692–2700, doi:10.1021/jp509839x.